Analysis of *Z–R* Relations Based on LDR Signatures within the Melting Layer

STEFAN KOWALEWSKI AND GERHARD PETERS

Max Planck Institute for Meteorology, Hamburg, Germany

(Manuscript received 17 July 2009, in final form 16 April 2010)

ABSTRACT

The inclusion of polarimetric measurements for the quantitative precipitation estimation (QPE) by weather radars as well as space- and airborne radars is considered most promising now-a-days. Because the melting layer region is usually marked by a distinct peak of the linear depolarization ratio (LDR), a possible correlation between LDR peak values and underlying drop sizes in terms of the *Z–R* relation is investigated, that is, the empirical relation between radar reflectivity factor *Z* and rain rate *R*. For this purpose, data taken during the Convective and Orographically Induced Precipitation Study (COPS) campaign in 2007 from two vertically pointing radars—a 24.15-GHz Micro Rain Radar (MRR) and a 35.5-GHz polarimetric cloud radar—were analyzed.

In this analysis a correlation between parameters of the *Z–R* relation and LDR peak values are revealed, implying that the LDR magnitude within the melting layer must be influenced by the size of melting particles. Furthermore, an LDR classification scheme shows an improvement of *R* retrieval with respect to the global *Z–R* relation optimized for the dataset herein. However, to asses the impact for improved QPE in the abovementioned applications, future research is necessary.

1. Introduction

Weather radars play an essential role in the quantitative precipitation estimation (QPE), which is a fundamental basis for various applications, such as flood forecasting or weather modeling (Meischner 2005). The capability of a single weather radar to monitor large areas at high spatial (less than a kilometer) and high temporal (about a minute) resolution makes it superior to local measurements. On the downside, the rain-rate retrieval by weather radars relies on an empirical relation to the received power of backscattered radar echoes, which strongly depends on the drop size distribution (DSD) of interfering hydrometeors. Because the DSD is subject to great variability, this causes, among other sources of error, great uncertainty to the rain-rate retrieval; therefore, additional information is needed to allow useful rain-rate estimates.

Early attempts to classify relations between the reflectivity factor *Z* and rain rate *R* are based on the detectability of the melting layer in the radar reflectivity profiles (Ulbrich and Atlas 2002).

In case of a vertically pointing direction, DSDs can be retrieved from the Doppler spectra as proposed by Atlas et al. (1973). While this pointing direction provides only local measurements for stationary radar setup, the method suffers from Doppler broadening in air- and spaceborne applications (Meneghini and Kozu 1990; Bolen and Chandrasekar 2000; Hildebrand et al. 1994).

To tackle these problems, the inclusion of polarimetric measurements from modern radars may be considered promising to improve rain-rate retrievals. In particular, the melting layer region of stratiform clouds can show strong signatures within parameters that are sensitive to depolarization (Kropfli et al. 1984). This motivates the idea of investigating whether these signatures can add valuable information to current rain-rate retrieval methods. Furthermore, this investigation may also contribute to our understanding of melting layer microphysics. It is worth mentioning that modeling the melting layer remains a challenging task and various modeling attempts can be found in the literature (e.g., Szyrmer and Zawadzki 1999; D'Amico et al. 1998; Russchenberg and Ligthart 1996).

Corresponding author address: Stefan Kowalewski, Bundesstraße 55, Max Planck Institute for Meteorology, Hamburg 20146, Germany.
E-mail: stefan.kowalewski@zmaw.de

DOI: 10.1175/2010JTECHA1363.1

This study focuses on the linear depolarization ratio (LDR) within the melting layer region. Measurements of LDR were retrieved by the cloud radar, type MIRA36, deployed in Achern, Germany, by the Meteorological Institute of the University of Hamburg (MI) and the Max Planck Institute for Meteorology (MPI) during the Convectively and Orographically Induced Precipitation Study (COPS; online at http://www.cops2007.de) in the summer of 2007. A Micro Rain Radar (MRR), which is capable of resolving DSDs from the radar signals, was deployed next to the cloud radar. Accordingly, we introduce an LDR classification scheme, which enables us to evaluate the impact of LDR values to the DSDs of precipitation. Furthermore, we investigate whether the inclusion of LDR values can be useful for improving the empirical relation between rain rate and radar reflectivity.

2. Instrumentation

a. Micro Rain Radar (MRR)

The MRR data that we analyze in this study were collected from a 24.15-GHz K-band frequency-modulated, continuous-wave (FM–CW) Doppler radar. It is a vertically pointing radar, which is capable of resolving DSDs from the retrieved Doppler spectra by using the relation between drop size and terminal fall velocity according to Atlas et al. (1973). Although the MIRA36 is also capable of resolving DSDs from its Doppler spectra, the larger dynamic range of the MRR makes it superior for the analysis of raindrops.

Vertical profiles of the DSD and other variables, such as the reflectivity factor Z and corresponding rain rate R (deduced from the DSD), are recorded with a temporal resolution of 60 s and a spatial resolution of 100 m, with a maximum range of 3100 m. A detailed discussion of the MRR can also be found in Peters et al. (2002, 2005).

b. MIRA36 cloud radar

The cloud radar data were retrieved from the vertically pointing MIRA36 K_a-band Doppler radar, which operates at 35.5 GHz. In contrast to the MRR, this radar is equipped with a polarization filter and a second independent receiver channel for simultaneously receiving co- and cross-polarized return signals, making it capable of retrieving LDR measurements. Vertical profiles of LDR are retrieved with temporal resolution of 10 s and spatial resolution of 30 m, with a maximum range of more than 14 km. Further information is also available at the manufacturer's homepage (online at http://www.metek.de).

c. Error discussion

Because our analysis is based on correlations between measurements taken from both radars, we make the assumption that errors of both systems are independent from each other; that is, they will not cause an artificial correlation between both measurements. Therefore, we will just briefly address two noticeable error sources here; for a more detailed discussion on these error sources we refer to Peters et al. (2005, 2010).

One error source is caused by vertical wind fields that are associated with turbulence or convection, because this will affect the assumed relation between drop size and terminal fall velocity. However, this error source should be more relevant for convective rain rather than for considered stratiform rain.

Another error source is caused by the attenuation of the radar signal. For the MRR data, an attenuation correction algorithm has been applied, whereas for the MIRA36 data, any attenuation effects of the LDR should be negligible.

3. LDR classification scheme

a. LDR in the melting layer

The LDR analysis in this study focuses on the melting layer region, that is, the transition zone of melting hydrometeors from ice phase to liquid phase. In particular, stratiform rain events show distinct melting layer characteristics within the radar profiles.

By definition, the LDR is the ratio of the cross-polar signal power to the copolar signal power (Doviak and Zrnić 1993). A time–height profile of the LDR taken from MIRA36 is shown in Fig. 1b. Among other parameters, the LDR shows a significant peak within the vertical profile, which is traditionally believed to be due to the nonsphericity of melting hydrometeors and the enhanced refractive index caused by water coating (Houze 1994). Accordingly, the LDR is primarily discussed in the literature as a shape-sensitive measurand, whereas the target size dependency seems to play a minor role (Bringi and Chandrasekar 2001). However, by taking the departure from the Rayleigh condition into account the question arises whether the increase in target size (e.g., resulting from target aggregation within the melting layer) might significantly enhance the target shape effect to the incident radar signal. Furthermore, in situ measurements within ice clouds revealed a significant correlation between target size and departure from ''target roundness'' (Korolev and Isaac 2003). Both arguments motivate the idea that a possible correlation might exist between the LDR peak values (LDR_P) within the melting layer and the underlying raindrop sizes. Thus, we consider whether LDR_P is one candidate to classify coefficients of the Z–R relation.

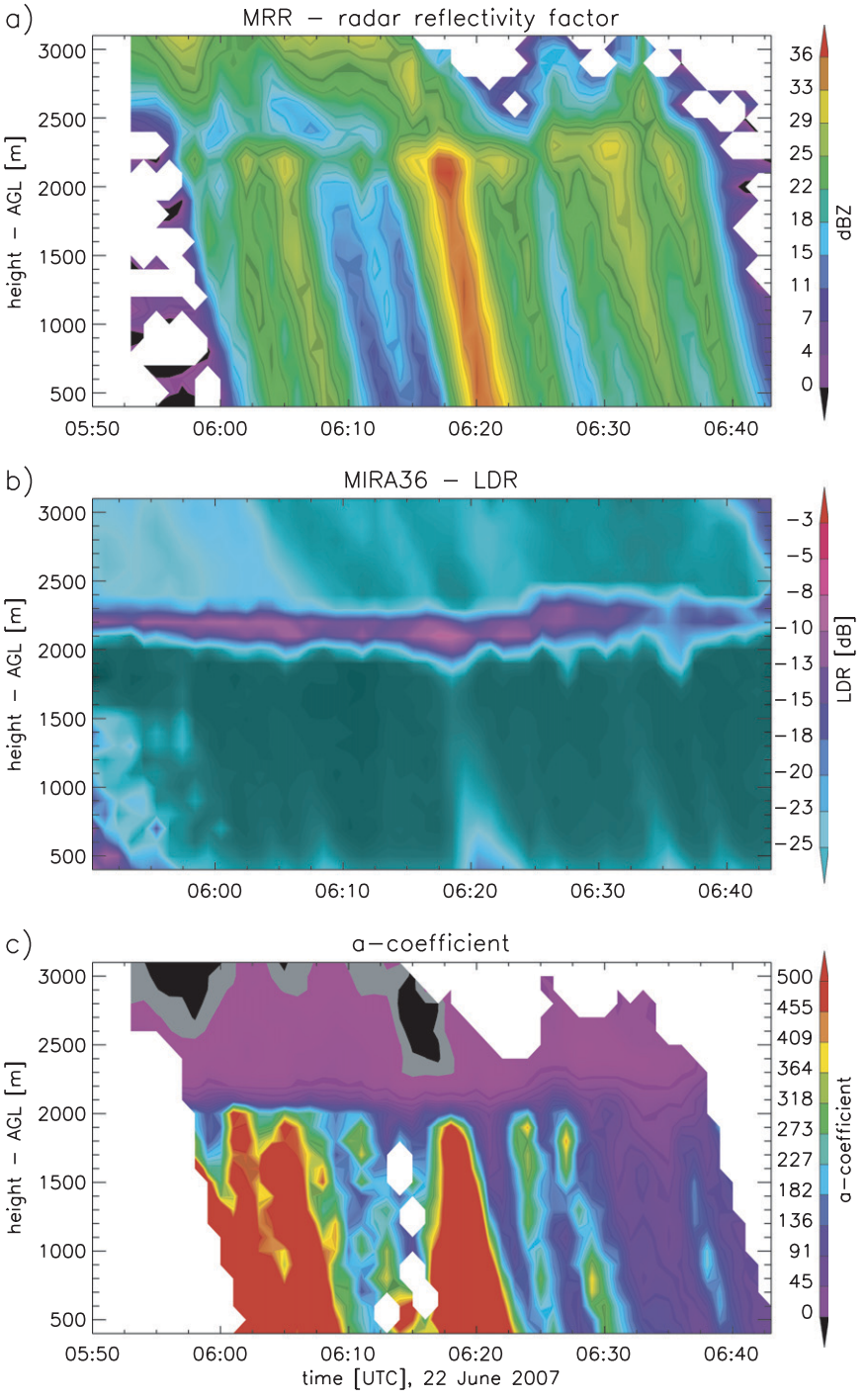

FIG. 1. (a) The MRR time–height profiles (above ground level) of the reflectivity factor Z for 22 Jun 2007. (b) The corresponding LDR profile taken from the MIRA36. (c) The time–height profile of the a coefficient derived from $a = Z/R^{1.4}$.

b. *Characteristic drop size*

The relation between the coefficients of a Z–R relation

$$Z = aR^b \tag{1}$$

and the DSD as function of rain rate has been discussed in depth by Steiner and Smith (2004). For a qualitative interpretation of the a and b coefficients based on this discussion, we consider Z as a function of DSD, as

$$Z = \int_{D=0}^{D=\infty} N(D) D^6 \, dD. \quad (2)$$

Here, $N(D)$ denotes the number of drops with diameter between D and $D + dD$. If we assume that the shape of DSD remains fixed, any change of $N(D)$ in Eq. (2) results in a constant factor. Therefore, we have a linear response between Z and R for a fixed DSD shape, corresponding to $b = 1$ in Eq. (1). Consequently, the a coefficient of the Z–R relation is a purely drop size–controlled parameter. On the other hand, if we allow the shape of DSD to change with rain rate, we account for this with the b coefficient in Eq. (1). Therefore, we interpret the b coefficient as a measure of the change of DSD shape with varying rain rate.

Based on this consideration, we will use the a coefficient of Eq. (1) as a characteristic measure of drop size within the DSD.

c. Coefficient retrieval

Transformation of Eq. (1) into logarithmic domain results in a linear equation,

$$\log(Z) = a_{\log} + b_{\log} \log(R), \quad (3)$$

with $a_{\log} = \log(a)$ and $b = b_{\log}$. This allows us to determine both coefficients by linear regression for a given sample of Z and R values. However, the evaluation of this regression from measurements usually results in large scattering with increasing sample number because of either temporally or spatially inhomogeneous rainfall. To illustrate the inhomogeneity of the Z–R relations within rainfall profiles, we set the b coefficient to a fixed value. This enables us to unambiguously retrieve an a coefficient for each single Z–R pair, where Z and R are derived from the corresponding DSD.

Figure 1 shows a time–height cross section of Z and the corresponding a coefficient cross section. Slanted trails are clearly visible in both profiles, where high a coefficient trails precede high reflectivity trails. Because high a coefficients reflect the presence of large raindrops according to our consideration, this finding reveals the drop-sorting effect within the observed rainfall event. On the other hand, the slanting underlines another problem with respect to the analysis of vertical profiles. Apparently, the correlation between two independent measurements—one being taken within the melting layer and the other being taken below—is affected by the vertical distance between them. Hence, a best correlation is expected at closest distances to the melting layer.

d. Analysis

The scheme that we choose to investigate a possible correlation between the a coefficient and LDR values within the melting layer relies on a classification of vertical Z and R profiles according to their corresponding LDR_P values. To assign each profile with an LDR_P value, if it exists, we resampled the MIRA36 data down to the time and height resolution of the MRR data. Furthermore, a melting layer detection algorithm, which analyzes enhancements in the vertical reflectivity and LDR profiles, as well as enhancements in the Doppler velocity gradient (Bumke et al. 2006), must have found a melting layer close to the LDR_P height, or the Z and R profiles are discarded from the analysis. According to our dataset, this selection criterion reduces the rain data by 20%.

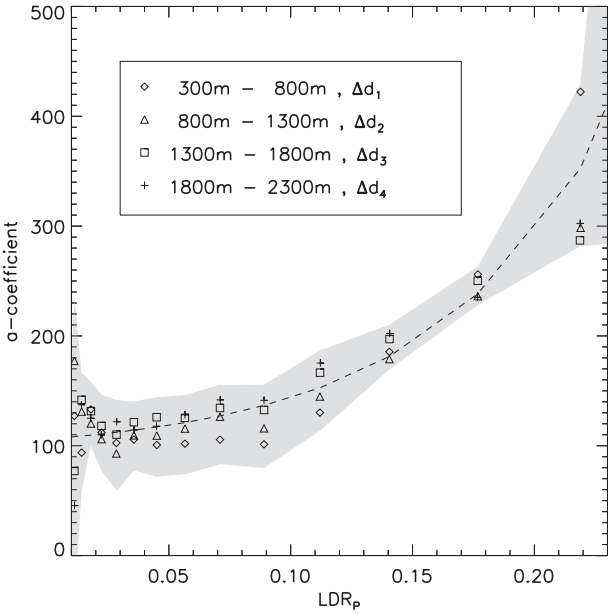

FIG. 2. The a coefficients as function of LDR_P class and four LDR peak distance ranges Δd_i; 95% prediction bands for a coefficients (maximum with respect to d) are indicated (gray shading). An exponential fit of the a coefficients is indicated (dashed line).

For a period of 92 days, starting from 1 July 2007, we assign each profile to the corresponding LDR_P value. Then, we define LDR_P classes that are binned by 1-dB increments. Accordingly, each LDR_P class contains a set of Z and R values. In the next step, we select samples of Z and R pairs from these sets according to the corresponding distances d to the LDR peak height. From these subsets we could already retrieve the a and b coefficients as functions of d and LDR_P by evaluating Eq. (3). However, we modified this regression analysis to a neutral regression analysis, because we do not see any obvious reason why we should prefer to set either Z or R as a dependent variable. Once we have evaluated the neutral regression coefficients for each subset, we look for a possible correlation between the regression coefficients and corresponding LDR_P classes.

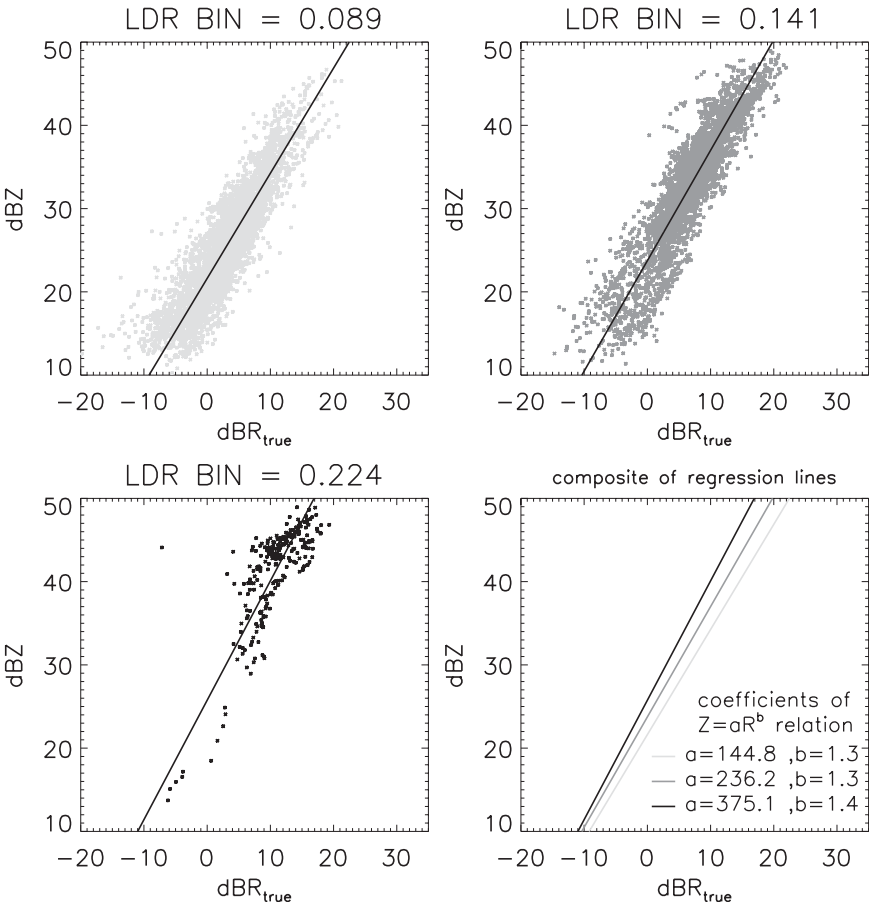

FIG. 3. Three *Z–R* scatterplots of different LDR_P classes, where *d* is ranging from 800 to 1300 m. The neutral linear regression is denoted (solid line), and a composite plot of all lines is shown in the lower-right plot.

4. Results

a. Correlation analysis

The retrieved *a* coefficients for each LDR_P class, with *d* values ranging from 300 to 2300 m, are presented in Fig. 2. Here we averaged the *a* coefficient over layers of 500 m. Because each *a* coefficient results from a neutral regression analysis, we evaluated its 95% prediction band. The maximum prediction bands for each *d* are indicated by gray shades in Fig. 2.

A positive correlation exists between *a* coefficients and LDR_P values beginning at about $LDR_P = 0.09$ (linear units). The large scattering at the highest LDR_P class can be explained by the decreasing population size, which also becomes apparent in a broadening of the prediction bands. Furthermore, the order of *a* coefficients with respect to *d* is flipping at about the 0.175 LDR_P class. However, we cannot decide at this point to what extent this reflects a microphysical process on the fall path or statistical artifacts.

The question arises whether the observed correlation between LDR and *a* may be mainly related to the drop-sorting effect. Because drop sorting evolves on the fall path, we would also expect a dependence of the prediction interval on *d*. Nevertheless, no significant dependence of individual prediction bands (not shown) on *d* was observed. Hence, we believe that the correlation is less influenced by the drop-sorting effect.

b. Z–R sets

To get a better sense for the *Z–R* subsets that we select in our analysis, we include three *Z–R* scatterplots in Fig. 3. Each scatterplot belongs to a specific LDR_P class, while a composite plot of corresponding regression lines is shown in the lower-right plot. Again, we can see that the intercept of the regression lines (i.e., *a* coefficient) is moving upward for higher LDR_P classes. Referring back to the idea that the inclusion of polarimetric parameters may contribute to the rain-rate retrieval, we might ask whether the *Z–R* subsets show a better agreement for

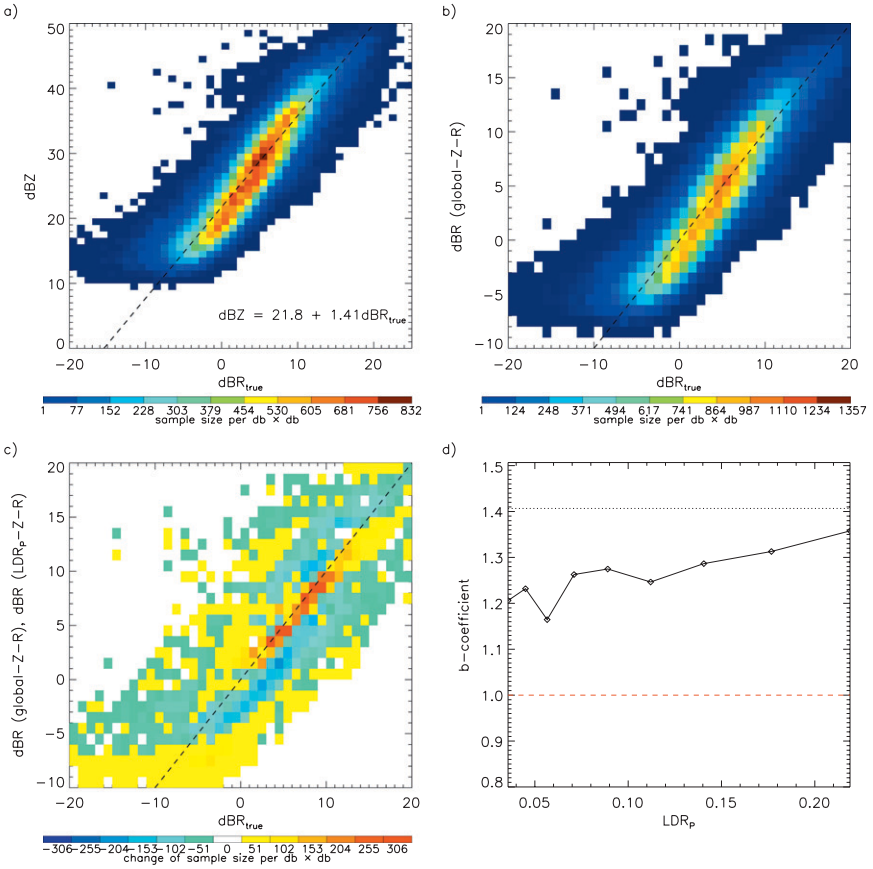

FIG. 4. (a)–(c) 2D histograms. (a) The global Z–R population; the independent linear regression is denoted (dashed line). (b) A comparison between rain rates derived from the global Z–R relation (ordinate) and "true" rain rates derived from the DSD (abscissa); the ideal match line is denoted (dashed line). (c) Population losses and gains with respect to (b) if rain rates are derived from Z–R relations as function of LDR$_P$ class instead of the global Z–R relation. (d) Derived b coefficients of considered LDR$_P$ range. Unity (red dashed line) and b coefficients of the global population (black dotted line) are denoted.

a linear regression model than the total set of Z–R will do.

c. *Improvement of Z–R relation*

To assess this question, we compare rain rates retrieved from a global Z–R relation (optimized for this dataset) with rain rates retrieved from Z–R relations of subsets according to our LDR classification scheme. For this part of the analysis, we restrict the global population of Z and R pairs to a corresponding LDR$_P$ range from 0.03 to 0.22, with d ranging from 300 to 2300 m.

As previously mentioned, the MRR retrieves rain rates directly from the DSD; hence, we denote these rain rates as "true" rain rates (R_{true}) in the following. Figure 4a shows a 2D histogram of the global Z–R_{true} sample and its neutral linear regression based on Eq. (3), which represents the optimized global Z versus R_{true} relation. If we evaluate the rain rates from the reflectivity factor and the global Z–R_{true} relation, a comparison with true rain rates shows large scattering (Fig. 4b). Instead of using this global Z–R relation for the rain-rate retrieval, we determine conditional Z–R relations for each LDR$_P$ class in the next step. The comparison between true rain rates and retrieved rain rates from the conditional Z–R relations reveals that large scattering persists (not shown). However, a noticeable rise of population appears at the ideal match line, which is denoted by the dashed line in Figs. 4b,c. To visualize this effect, we subtract the population sizes of Fig. 4b from the population sizes corresponding to conditional Z–R relations. The color-coded losses and gains are shown in Fig. 4c. As can be seen, noticeable gains (indicated by red) occur at the ideal match line, but similar losses (indicated by blue) also occur in adjacent domains, indicating an improvement to the Z–R evaluation method according to LDR$_P$ classes. On the other hand, large domains of small changes exist,

which do not significantly deplete outliers in Fig. 4b. Despite the noticeable accumulation of samples in close vicinity to the ideal match line (15% increase for 0-dB R_{true} to 12-dB R_{true}) in Fig. 4c, we failed to find a suitable statistic parameter showing a significant improvement.

Finally, in Fig. 4d we show that the conditional *b* coefficients are closer to unity than the global *b* coefficient, which indicates that our selection of *Z–R* pairs prefers DSDs with constant shapes.

5. Discussion and conclusions

This study reveals two findings. First, the positive correlation that we found between LDR_P values and *a* coefficients suggests that high LDR values within the melting layer is size controlled rather than purely shape controlled. This supports the modeling results of Tynnelä et al. (2009), who state that the increase in LDR with size is due to the increased impact of particle shape on scattering with increased size parameters as the Rayleigh-type behavior starts to diminish.

The second finding is the observed improvement of the global *Z–R* relation by the LDR_P classification scheme. However, in terms of statistical significance, we can only state a small improvement so far. One problem might be the diminishing causality with fall depth between *Z–R* pairs and their assigned LDR_P values resulting from the slanted rain trails in the time–height profiles. Apart from this problem, further questions need to be addressed before our findings could be transformed to applications with grazing scanning angles. For example, the impact of partial attenuation needs to be investigated.

On the other hand, the K-band radar that is to be mounted on the High Altitude and Long Range Research Aircraft (HALO; Mech et al. 2009) this year will be an interesting testing ground for our classification scheme. In addition to LDR, other polarimetric parameters in the melting layer might provide valuable information as well for *Z–R* classification in analogy to the proposed scheme.

Acknowledgments. This study was supported by Contract VI_156 DLR 06–330 of the Helmholtz Society and DFG project Towards Optimal-Estimation-Based Snow Characterization Algorithm (TOSCA). We thank Sabrina Melchionna, Marco Clemens, and Matthias Bauer for discussions, suggestions, and proofreading. Hans Münster prepared the experimental setup and took care of the measurements.

REFERENCES

Atlas, D., R. C. Srivastava, and R. S. Sekhon, 1973: Doppler radar characteristics of precipitation at vertical incidence. *Rev. Geophys.,* **11,** 1–35.

Bolen, S. M., and V. Chandrasekar, 2000: Quantitative cross validation of space-based and ground-based radar observations. *J. Appl. Meteor.,* **39,** 2071–2079.

Bringi, V. N., and V. Chandrasekar, 2001: *Polarimetric Doppler Weather Radar*. 1st ed. Cambridge University Press, 636 pp.

Bumke, K., M. Clemens, H. Graßl, S. Pang, G. Peters, J. E. E. Seltmann, T. Siebenborn, and A. Wagner, 2006: More accurate areal precipitation over land and sea. Max Planck Institute for Meteorology, Reports on Earth System Science, Tech. Rep. 22, 67 pp. [Available online at http://www.mpimet.mpg.de/fileadmin/publikationen/Reports/BzE_22.pdf.]

D'Amico, M. M. G., A. R. Holt, and C. Capsoni, 1998: An anisotropic model of the melting layer. *Radio Sci.,* **33,** 535–552.

Doviak, R. J., and D. S. Zrnić, 1993: *Doppler Radar and Weather Observations*. Academic Press, 562 pp.

Hildebrand, P. H., C. A. Walther, C. L. Frush, J. Testud, and F. Baudin, 1994: The ELDORA/astraia airborne Doppler weather radar: Goals, design, and first field tests. *Proc. IEEE,* **82,** 1873–1890.

Houze, R. A., 1994: *Cloud Dynamics*. Academic Press, 573 pp.

Korolev, A., and G. Isaac, 2003: Roundness and aspect ratio of particles in ice and clouds. *J. Atmos. Sci.,* **60,** 1795–1808.

Kropfli, R. A., W. R. Moninger, and F. Pasqualucci, 1984: Circular depolarization ratio and Doppler velocity measurements with a 35-GHz radar during the cooperative convective precipitation experiment. *Radio Sci.,* **19,** 141–147.

Mech, M., G. Peters, S. Crewell, L. Hirsch, and T. Rose, 2009: HAMP—The microwave package on the upcoming High Altitude and Long Range Aircraft HALO. *Proc. Fourth IPWG Workshop,* Beijing, China, ISAC/CNR, 261–267.

Meischner, P., Ed., 2005: *Weather Radar: Principles and Advanced Applications*. 2d ed. Springer, 337 pp.

Meneghini, R., and T. Kozu, 1990: *Spaceborne Weather Radar*. Artech House, 199 pp.

Peters, G., B. Fischer, and T. Andersson, 2002: Rain observations with a vertically looking Micro Rain Radar (MRR). *Bor. Environ. Res.,* **7,** 353–362.

——, ——, H. Münster, M. Clemens, and A. Wagner, 2005: Profiles of raindrop size distributions as retrieved by microrain radars. *J. Appl. Meteor.,* **44,** 1930–1949.

——, ——, and M. Clemens, 2010: Rain attenuation of radar echoes considering finite range resolution and using dropsize distributions. *J. Atmos. Oceanic Technol.,* **27,** 829–842.

Russchenberg, H. W. J., and L. Ligthart, 1996: Backscattering by and propagation through the melting layer of precipitation: A new polarimetric model. *IEEE Trans. Geosci. Remote Sens.,* **34,** 3–14.

Steiner, M., and J. A. Smith, 2004: A microphysical interpretation of radar reflectivity–rain rate relationships. *J. Atmos. Sci.,* **61,** 1114–1131.

Szyrmer, W., and I. Zawadzki, 1999: Modeling of the melting layer. Part I: Dynamics and microphysics. *J. Atmos. Sci.,* **56,** 3573–3592.

Tynnelä, J., T. Nousiainen, S. Göke, and K. Muinonen, 2009: Modeling C-band single scattering properties of hydrometeors using discrete-dipole approximation and *T*-matrix method. *J. Quant. Spectrosc. Radiat. Transfer,* **110,** 1654–1664, doi:10.1016/j.jqsrt.2009.02.020.

Ulbrich, C. W., and D. Atlas, 2002: On the separation of tropical convective and stratiform rains. *J. Appl. Meteor.,* **41,** 188–195.